Tight-binding calculations of the Ni-Al phase diagram

C. Colinet, P. Hicter, and A. Pasturel
Laboratoire de Thermodynamique et Physico-Chimie Métallurgiques,
Ecole Nationale Supérieure d'Electrochimie et d'Electrométallurgie de Grenoble, Boîte Postale 75,
38402 Saint Martin d'Heres, France
(Received 1 May 1991)

Tight-binding electronic band-structure calculations were combined with a free-energy expression given by the cluster-variation method. The effective pair interactions used in the cluster-variation method were evaluated by the cluster-Bethe-lattice method. They are restricted to the first-nearest neighbors in fcc-based structures and to first- and second-nearest neighbors in bcc-based structures; *s* and *d* orbitals have been used for Ni, while *s* and *p* orbitals were included for Al. The phase diagram has been constructed incorporating both fcc and bcc lattices and the occurring ordered compounds. The liquid part has been evaluated using the same Hamiltonian, chemical short-range order being calculated in an isotropic environment. The calculated diagram agrees reasonably well with the one determined experimentally.

I. INTRODUCTION

In the past decade, it has been a goal to combine at a high level of accuracy both quantum-mechanical and statistical-thermodynamical contributions to obtain a theoretical knowledge of the phase diagrams. One of the most efficient statistical-mechanics techniques is the cluster-variational method[1] (CVM), which provides a good description of the free energy as a function of short-range order (SRO). The CVM requires, as input, interaction parameters that determine ordering or clustering reactions occurring in the alloy systems. These interactions must be defined carefully and then obtained by means of quantum-mechanical calculations. The realization that these interactions can be derived from electronic band-structure calculations has initiated extensive research in this field. At the present time, two approaches are available for such calculations. The first one is the so-called Connolly-Williams[2] and the closely related εG, approach;[3] in this approach it is assumed that the total energy can be written as a sum of configuration-independent many-body interaction potentials multiplied by the multisite correlation functions. The sum runs over all the cluster types and in practice, it requires the existence of a maximum cluster beyond which the many-body interactions are supposed to be negligible. In the second approach, the energy of the completely disordered solid solution is calculated by the coherent-potential approximation (CPA).[4] The effective-cluster interactions are calculated by the embedded-cluster method[5] or by the generalized perturbation method[6] (GPM) using a perturbative treatment about the completely disordered state. In this case, the ordering energies can be written as an expression in terms of concentration-dependent *n*th-order effective-cluster interactions. The GPM can be developed with the first-principles multiple-scattering formalism of the Korringa-Kohn-Rostoker coherent-potential approximation,[7] or more simply in the framework of the tight-binding approximation (TBA).[8] At this level of approximation, let us also mention the alternative approach proposed by Robbins and Falicov[9] and which is called the alloy cluster-Bethe-lattice method (CBLM). Despite the fact that the CBLM relies on a topological approximation that replaces the real crystal lattice with a Cawley tree, this approach has the great advantage that it includes SRO explicitly in the calculation of the electronic spectrum and internal energy. Contrary to the TB-GPM-CPA calculations,[10] the effect of charge-transfer on SRO is taken into account, a contribution which has been shown by Robbins and Falicov[11] to be of consequence in the variation of energy with SRO. But perhaps the most interesting aspect of this approach is that the study of SRO can be extended to topologically disordered systems, such as amorphous or liquid materials, using the scalar cluster-Bethe-lattice approximation.[12] Thus it allows one to treat on the same footing the solid and the liquid part of the phase diagram due to the same level of approximation used in both calculations. This is in fact a necessary condition for the study of equilibrium between liquids and compounds or solid solutions.

In this paper we have focused our attention on the relatively complex Ni-Al system which is of both theoretical and technological importance. Sigli and Sanchez[13] have shown that a CVM treatment using effective-pair interactions (EPI) determined from available thermochemical data was able to give a good representation of the phase diagram. Our purpose is thus to calculate these effective-pair interactions using more elaborate quantum-mechanical calculations. In a previous paper,[14] calculations of the electronic structure of Ni-Al compounds and the subsequent study of hybridization effects on thermodynamic properties have been presented in the framework of a tight-binding approximation coupled with CBLM. EPI have been extracted, using that alloy energy could be well represented by a function consisting of a nonlocal term describing the energy of the random alloy and an ordering term given by concentration-dependent EPI. Their manifestation on the phase diagram determination via the tetrahedron approximation of the CVM is now presented.

The paper is organized as follows. In Secs. II and III we present a brief review of the quantum- and statistical-mechanical approaches used in our calculations. In Sec.

 ©1992 The American Physical Society

IV we present the results of the calculations for the Ni-Al system and compare them with the available experimental data.

II. MODEL

A. The tight-binding bond model

The main assumptions of the model used by Nguyen Manh *et al.*;[15] Pasturel, Nguyen Manh, and Mayou,[16] and more recently by Colinet, Bessoud, and Pasturel[14] to calculate the electronic properties of T-Al compounds are briefly reviewed here. We choose as the Hamiltonian a tight-binding Hartree model with intersite and intrasite electron-electron Coulomb interactions, neglecting the magnetic interactions,

$$H=\sum_{i\mu} E_{i\mu}|i\mu\rangle\langle i\mu| + \sum_{i\mu,j\nu} t_{i\mu,j\nu}|i\mu\rangle\langle j\nu| + H_{\text{ion-ion}} - H_{e\text{-}e} \ . \tag{1}$$

The first two terms represent the one-electron Hamiltonian H_{1e}, incorporating the effective potential from the ions and other valence electrons. $H_{e\text{-}e}$ is a correction for counting the electron-electron interaction in H_{1e} twice and $H_{\text{ion-ion}}$ represents the ion-ion interaction. In this expression, $|i\mu\rangle$ is the ket for the orbital μ on site i, the on-site and hopping energies $E_{i\mu}$ and $t_{i\mu,j\nu}$ give, respectively, the effective atomic energy of the μ orbital on site i and its coupling to the orbital ν on site j.

In our calculations we assume that the on-site and hopping energies, i.e., $E_{i\mu}$ and $t_{i\mu,j\nu}$, depend only on the species of atom at the relevant sites and in the case of hopping parameters, the relative positions of the sites

$$\begin{aligned} E_{i\mu} &= E^0_{I\mu} + \psi_{I\mu} \ , \\ t_{i\mu,j\nu} &= t_{I\mu,J\nu}(r) \ , \end{aligned} \tag{2}$$

where I denotes the species I at site i, $t_{I\mu,J\nu}(r)$ and $E^0_{I\mu}$ are intrinsic tight-binding parameters, and $\psi_{I\mu}$ is the mean effective Coulomb potential seen by the μ orbital on a type-I atom in a given alloy, which is calculated in two parts: an intrasite contribution (effective direct exchange energy) $\psi^{\text{intra}}_{I\mu}$, and an intersite contribution (effective Madelung energy).

The one-electron total energy E_{1e} is given simply by integrating up to the Fermi energy E_F the density of electronic states $N(E)$ multiplied by the energy E,

$$E_{1e}=\int_{-\infty}^{E_F} N(E)E\,dE \ . \tag{3}$$

The intra-atomic electron-electron energy can be approximated by[17]

$$E^{\text{intra}}_{e\text{-}e}=\tfrac{1}{2}\sum_{I\mu,\nu} x_I U_{\mu,\nu}\langle n_{I\mu}\rangle\langle n_{I\nu}\rangle \ , \tag{4}$$

where x_I is the concentration of I species at site i, and $U_{\mu,\nu}$ the effective intrasite Coulomb interactions,

$$\langle n_{I\mu}\rangle=\int^{E_F} N_{I\mu}(E)\,dE \tag{5}$$

and

$$n_I=\sum_{\mu}\langle nI_{\mu}\rangle \ . \tag{6}$$

As shown by Robbins and Falicov[18] the electron-electron and ion-ion intersite interactions can be written as

$$E^{\text{inter}}_{\text{ion-ion}} - E^{\text{inter}}_{e\text{-}e} = -V(Z/2)\sum_I x_I \sum_J P_{IJ}(n_I n_J - n^0_I n^0_J) \ , \tag{7}$$

where V denotes the nearest-neighbor contribution to the average intersite potential per transferred electron, $\Delta n_I = n_I - n^0_I$ is the charge transfer to species I, Z is the coordination number, and P_{IJ} describes the pair probabilities.

B. The electronic density of states in the alloy

A quantity which is of central interest in our calculations is the electronic density of states. According to the state which characterizes the alloy at a given composition, i.e., liquid state, solid solution, or compound, three different steps are required to calculate the electronic density of states of the alloy.

1. Compounds

To calculate the electronic density of states of compounds, we have used the recursion method,[19] which constructs a new orthogonal basis $\{|\xi k\rangle, k=1,\ldots\}$ from the linear combination of atomic orbitals (LCAO) orthogonal basis $\{|i\mu\rangle\}$, where the tight-binding Hamiltonian matrix is tridiagonal. If $|\xi 1\rangle$ is made equal to $|i\mu\rangle$, then the Green's function of this Hamiltonian is given by the continued fraction

$$\langle i\mu|G(z)|i\mu\rangle = \cfrac{1}{z-a_1-\cfrac{b_1^2}{z-a_2-\cfrac{b_2^2}{z-a_3\cdots}}} \ , \tag{8}$$

where $\{a_n\}$ and $\{b_n\}$ are the matrix elements.

The coefficients a_n and b_n^2 are calculated up to a given step n_0 and the continued fraction is then terminated in the usual way: $a_{n>n_0}=a_\infty$ and $b^2_{n>n_0}=b^2_\infty$.[10] We repeat these calculations for all the nonequivalent sites of the compound studied and the electronic density of states of the compound is given by the sum of these local densities of states.

2. Solid solutions

To compute the electron density of states of a solid solution which can exhibit chemical short-range order, we have used the alloy cluster-Bethe-lattice method in its simplest version; i.e., a single-atom cluster. The real lattice is replaced by a Bethe lattice and the configurations of the environment of an atom are treated in a mean-field approximation. Within this scheme, the coordination number and mean distribution of the nearest neighbor are reproduced exactly.

The mean Green's function of atom I on site i is given by the CBLM equations,[12]

$$G_I(z)=\frac{1}{z-H_{0I}-\sum_{R_K,J} P_{JI}T_{JI}^{\dagger}(R_K)G_J(z,R_K)T_{JI}(R_K)} , \tag{9}$$

$$G_I(z,R_K)=\frac{1}{z-H_{0I}-\sum_{J,R_L\,(\neq -R_K)} P_{JI}T_{JI}^{\dagger}(R_L)G_J(z,R_L)T_{JI}(R_L)} , \tag{10}$$

where $T_{JI}(R_K)$ is the transfer matrix from an I atom to a J atom in direction R_K, and $G_J(z,R_K)$ is the mean Green's function of a J atom located on the auxiliary Bethe lattice, which is obtained from the initial Bethe lattice by removing the bond in direction $-R_K$.

H_{0I} is the Hamiltonian without hybridization. Chemical short-range order (CSRO) appears in the definition of the pair probabilities and for each composition and degree of SRO, the density of states is computed self-consistently. The total energy is also calculated as a function of SRO; we shall see that its SRO dependence is particularly important since it is from this that the effective-pair interactions will be obtained.

3. *Liquid alloys*

Liquid alloys may also display CSRO, as has been shown very recently for the liquid $Al_{80}Ni_{20}$ alloy,[20] and it is essential to consider this when determining their thermodynamic quantities. The best way to perform such calculations is to use a variational method with, as a reference system, a mixture of hard spheres which all have the same diameter but different charges and which interact through a screened Coulomb potential.[21] This reference system has been found to describe well the structural and thermodynamic manifestations of ordering in disordered alloys.[22,23] To compute local density of states, we have used the scalar version of the alloy CBLM.[12]

The Green's function of atom I is given by

$$G_I(z)=\sum_{\alpha(I)} P_\alpha G_\alpha(z) . \tag{11}$$

$G_I(z)$ is scalar inside the invariant subspaces $\alpha(I)$ defined by the types of orbitals chosen (s, p, and d in our case),[12] and Eqs. (9) and (10) become

$$G_\alpha(z)=\frac{1}{z-H_{0\alpha}-\sum_{\beta}\sigma_{\alpha\beta}^2 G_\beta(z)} , \tag{12}$$

$$G_\beta(z)=\frac{1}{z-H_{0\beta}-\sum_{\alpha}\sigma_{\beta\alpha}^2 G_\alpha(z)} , \tag{13}$$

where $\sigma_{\alpha\beta}^2$ is the part of the mean second moment of the density of states (DOS) on a state α due to the coupling with states β of the neighbors, and

$$\sigma_{\alpha\beta}^2=\frac{1}{n_\alpha}\int d^3R\, g_{JI}(R)\,\mathrm{Tr}[T_{JI}^{+}(R)P_\beta T_{JI}(R)P_\alpha] , \tag{14}$$

where n_α is the degeneracy of the subspace α and $g_{JI}(R)$ the pair-correlation function between atoms of type I and J, provided by the reference system.

For liquid alloys, the electron-electron and ion-ion intersite interactions also have a particular expression;[13] Eq. (7) becomes

$$\begin{aligned} E_{\text{ion-ion}}^{\text{inter}}-E_{e\text{-}e}^{\text{inter}}=-2\pi\rho\Big[& x_A^2(2n_A\Delta n_A+\Delta n_A^2)\int_0^\infty g_{AA}(R)V(R)^2dR \\ & +2x_Ax_B(n_A\Delta n_B+n_B\Delta n_A+n_A\Delta n_B)\int_0^\infty g_{AB}(R)V(R)R^2dR \\ & +x_B^2(2n_B\Delta n_B+\Delta n_B^2)\int_0^\infty g_{BB}(R)V(R)R^2dR\Big] , \end{aligned} \tag{15}$$

ρ being the number density.

To describe the liquid state in these types of liquid alloys, it is also possible to take a Bethe lattice with a coordination number roughly equal to 12; in this case, to describe SRO the pair-correlation functions are replaced by the pair probabilities. It has been shown that for thermodynamic data, i.e., ΔE and ΔS, these two approaches give similar results.[24] Of course, in the second case, information about the structure of the liquid is lost.

C. Electronic parameters

The electronic parameters are similar to the ones used by Colinet, Bessoud, and Pasturel in their study of cohesive properties of the Ni-Al system.[14] The calculations include the five d-like and one s-like orbitals for Ni metal and the three p-like and one s-like orbitals for Al metal. The hopping energies between like species were evaluated from Harrison's solid-state table,[25] and hop-

ping energies between different species were calculated using Shiba's approximation.[26] For the on-site energies, we use the atomic on-site energies given by Herman and Skillman;[27] for transition metals, the values were calculated for one transition atom with the $d^{n+1}s$ configuration.[28] The values of $E_s^{Ni}, E_d^{Ni}, E_s^{Al}, E_p^{Al}$ are equal to -0.76, -2.27, -2.94, and $+2.27$ eV, respectively. The Coulomb energies were taken to be $U_{ss}=0.50$ eV, $U_{sd}=0.75$ eV, $U_{dd}=1.6$ eV, and $V=0.25$ eV with the fact that $U_{ss}=U_{pp}$.

From this set of tight-binding parameters, the internal energy of the alloys in their different topological configurations can be calculated, which is the first step towards the phase-diagram calculation.

III. PHASE-DIAGRAM CALCULATIONS

A. Effective-pair interactions

As discussed in the Introduction, the internal energies can be considered as the starting point of the phenomenological treatment of alloy phase equilibria by means of the CVM. To extract effective-pair interactions it is more convenient to write the energy of alloy formation as

$$\Delta E_f = E_{\text{rand}}(x) + E_{\text{ord}}(x,\sigma) , \tag{16}$$

where σ is the parameter describing CSRO. As previously used,[14] E_{rand} is a function of the point correlation function ξ_1

$$E_{\text{rand}}(x) = (A_0 + B_0\xi_1)(1-x_1^2) \tag{17}$$

and the ordering energy is

$$E_{\text{ord}}(x,\sigma) = \tfrac{1}{2}\sum_k Z_k V_k(\xi_2^{(k)} - \xi_1^2) , \tag{18}$$

where Z_k, V_k, and $\xi_2^{(k)}$ are, respectively, the coordination number, effective-pair interaction, and pair-correlation function for kth nearest neighbor. For fcc-based structures, E_{ord} can be written as

$$E_{\text{ord}} = 4x(1-x)(Z/2)V_1\sigma \tag{19}$$

and for bcc-based structures

$$E_{\text{ord}} = 4x(1-x)[(Z_1/2)V_1\sigma_1 + (Z_2/2)V_2\sigma_2] . \tag{20}$$

V_1 for fcc-based structures and both V_1 and V_2 for bcc-based structures are obtained from the short-range-order dependence of the calculated energy of mixing.[14]

B. Configurational entropy

In order to compute a phase diagram, we need to know the total free energy of the binary alloy in a given phase, its energy, and also its entropy of formation. In these calculations, we keep only the configurational contribution neglecting the vibrational one. In the present approach, we use different configurational entropy approximations depending on the nature of the phase being considered. As for the calculations of the electronic density of states, three families of phases are distinguished.

1. Stoichiometric compounds

In this case, the configurational entropy is taken equal to zero.

2. Solid solutions or ordered phases presenting an extended concentration range

The configurational entropy is described by means of the CVM. The CVM entropy is found to be given approximately by a sum of the partial cluster entropies.[29] The maximum cluster used in our study is the tetrahedron containing both first and second neighbors in the bcc lattice. In the tetrahedron approximation the entropy of a bcc disordered system is given by[14]

$$S_{\text{bcc}} = k_B \left[6\sum_{i,j,k,l} w_{ijkl}\ln w_{ijkl} - 12\sum_{i,j,k} t_{ijk}\ln t_{ijk} + 3\sum_{i,j} y_{ij}^{(2)}\ln y_{ij}^{(2)} + 4\sum_{i,k} y_{ik}^{(1)}\ln y_{ik}^{(i)} - \sum x_i \ln x_i \right] , \tag{21}$$

where w_{ijkl}, t_{ijk}, $y_{ij}^{(2)}$, $yy_{ik}^{(1)}$, and xi denote, respectively, the probability of finding tetrahedra, triangles, second-neighbor pairs, first-neighbor pairs, and points in the configuration given by their subscripts (i equals A or B in a binary alloy).

For the disordered fcc structure, we have

$$S_{\text{fcc}} = -k_B \left[2\sum_{i,j,k,l} w_{ijkl}\ln w_{ijkl} - 6\sum_{i,j} y_{ij}^{(1)}\ln y_{ij}^{(1)} + 5\sum_i x_i \ln x_i \right] . \tag{22}$$

The cluster probabilities are related by the following consistency relationships:

$$t_{ijk} = \sum_l w_{ijkl} , \tag{23a}$$

$$y_{ij}^{(2)} = \sum_{kl} w_{ijkl} , \tag{23b}$$

$$y_{ik}^{(1)} = \sum_{jl} w_{ijkl} , \tag{23c}$$

$$x_i = \sum_{jkl} w_{ijkl} . \tag{23d}$$

As mentioned above, the equilibrium state of the system and the degree of SRO in the alloy is obtained at any given composition and temperature by minimizing the configurational free energy. In the case of tetrahedron approximation, the minimization is conveniently carried out using the natural iteration method (NIM) developed by Kikuchi.[30] The configurational variables are chosen to be the tetrahedron probabilities w_{ijkl} subject to the normalization condition

$$\sum_{ijkl} w_{ijkl} = 1 . \tag{24}$$

The natural iteration (NI) equations used in the present

model have been presented elsewhere[13] and will not be repeated here.

For the case of an ordered phase present in a range of concentration, long-range order is described in the usual manner by means of sublattices reflecting the symmetry of the ordered structure. A given cluster may now consist of points in the crystal belonging to different sublattices and their probabilities must be distinguished accordingly (see Ref. 31 for more details).

3. *Liquid alloys*

As has already been mentioned, the determination of CSRO in liquid alloys may be performed using thermodynamic variational calculations based on the hard-sphere Yukawa (HSY) reference system.[21] The structural manifestations of ordering are modeled by a mixture of hard spheres all having the same diameter but opposite charges (while respecting the overall charge neutrality condition) which interact by a Coulomb or screened Coulomb (Yukawa) potential. In this system, the description of the atomic configuration requires three parameters which are the diameter of the hard sphere σ, the strength of the ordering potential at hard contact ε, and a screening constant K. In terms of the average and ordering potentials, the reference interactions are given by

$$\psi_{NN}(R)=\begin{cases}\infty, & R<\sigma\\ 0, & R>\sigma\end{cases}, \tag{25a}$$

$$\psi_{CC}(R)=\begin{cases}\infty, & R<\sigma\\ -\varepsilon\sigma\exp[-K(R-\sigma)]/R, & R>\sigma\end{cases}, \tag{25b}$$

$$\psi_{NC}(R)=0\ . \tag{25c}$$

Because of Eq. (25c) the three coupled integral equations of the mean-spherical approximation (MSA) decouple into two independent equations. One, with the closure conditions (to the Ornstein-Zernike equations)

$$h_{NN}(R)=-1,\quad R<\sigma\ , \tag{26a}$$

$$c_{NN}(R)=0,\quad R>\sigma \tag{26b}$$

describes the fluctuations in the mean number density and is identical to the Percus-Yevick equations for hard spheres, hence we know its analytical solution.[32] The second, with the closure conditions

$$h_{CC}(R)=0,\quad R<\sigma, \tag{27a}$$

$$c_{CC}(R)=\varepsilon\sigma\exp[-K(R-\sigma)]/Rk_BT,\quad R>\sigma \tag{27b}$$

describes the local fluctuations in the compositions. Its analytical solution has been given by Waisman.[33] Within this reference system, the variational conditions become

$$\left.\frac{\partial F}{\partial\sigma}(\sigma,\varepsilon,K)\right|_{T,\rho,\varepsilon,K}=0\ ,$$
$$\frac{\partial F}{\partial\varepsilon}(\sigma,\varepsilon,K)|T,\rho,\sigma,K=0\ , \tag{28}$$
$$\frac{\partial F}{\partial K}(\sigma,\varepsilon,K)|T,\rho,\sigma,\varepsilon=0\ ,$$

with the variational upper bound to the exact free energy

$$F(\sigma,\varepsilon,K)=\tfrac{3}{2}k_BT+E_T(\sigma,\varepsilon,K)-T[S_{\rm HS}(\sigma)+S_{\rm ord}(\sigma,\varepsilon,K)]\ . \tag{29}$$

Explicit expressions for the roman HS and the ordering contributions to the entropy ($S_{\rm HS}$ and $S_{\rm ord}$) are given in Refs. 21 and 23. As we are interested in the occurrence of CSRO, we give here the expression of $S_{\rm ord}$

$$S_{\rm ord}=[f(w)-f(0)]/2\eta\ , \tag{30}$$

where η is the hard-sphere packing fraction and is equal to $\frac{1}{6}\rho\pi\sigma^3$, and the function $f(w)$ is given by

$$f(w)=-\frac{B_1+B_2+B_3^2}{72B_4^2(1+B_4w)^3}\ , \tag{31}$$

with

$$B_1=K\sigma\left[\frac{2}{\exp(K\sigma)-1}-1\right], \tag{32a}$$

$$B_2=-\tfrac{3}{2}[1-3\exp(-K\sigma)]\ , \tag{32b}$$

$$B_3=\exp(-K_\sigma)[1-\exp(-K\sigma)]/4K\sigma\ , \tag{32c}$$

$$B_4=[1-\exp(1-K\sigma)]/2K\sigma\ , \tag{32d}$$

and w is just twice the ratio between the ordering energy and the strength of the ordering potential at contact.

Also the reference HSY system provides expressions for partial pair-correlation functions $g_{IJ}(R)$, which allows us to define the structure of the liquid state and which enters the calculation of the internal energy [see Eqs. (14) and (15) and also the expression for the ordering contribution to the entropy]. An equivalent approach which is not discussed here[24] is the approximation of the liquid state by a Bethe lattice, using an isotropic environment to calculate internal energy. In this case, the coordination number Z and the Warren-Cowley parameter σ are the relevant parameters but their relation with HSY parameters can be established in the following way:

$$Z=\rho\int_0^{R_M}g_{NN}(R)4\pi R^2dR \tag{33a}$$

and

$$\sigma=\frac{\int_0^{R_M}g_{cc}(R)4\pi R^2dR}{\int_0^{R_M}g_{NN}(R)4\pi R^2dR}\ , \tag{33b}$$

where R_M is the radial distance corresponding to the first minimum of $g_{NN}(R)$.

For the ordering contribution to the entropy, it has been shown[24] that the expression of the disordered fcc structure [see Eq. (22)] displays trends of ordering which gives the better agreement with the one provided by the HSY expression. This approach presents the advantage of having only one parameter, i.e., s, to describe CSRO but, of course, structural information such as pair-correlation functions are lost now since the structure is described by a Bethe lattice characterized by the coordination number Z.

C. Phase equilibrium

In order to determine the equilibrium phase diagram, it is more convenient to minimize the grand potential Ω given by

$$\Omega = F - \mu \xi_1 , \tag{34}$$

where μ is the effective chemical potential. In the present work, the minimization of the grand potential is carried out with respect to a set of independent configuration variables. As has already been mentioned, this minimization is done using the NI method developed by Kikuchi.[30,31] In the use of the tetrahedron approximation, these configurational variables are chosen to be the tetrahedron probabilities w_{ijkl} at constant temperature T and effective potential chemical potential μ, taking into account the normalization constraint of Eq. (24).

The equilibrium phase diagram between two phases I and II is computed using the same scheme as proposed by Kikuchi and Murray.[34] For the same initial value of the effective chemical potential μ, the grand potentials of phases I (Ω_I) and II (Ω_{II}) are calculated using the procedure described above. If $\Omega_I = \Omega_{II}$ the equilibrium conditions are realized but if not, the value of μ is modified until $\Omega_I = \Omega_{II}$.

IV. RESULTS FOR THE Ni-Al SYSTEM

The Ni-Al phase diagram displayed in Fig. 1 is characterized by a liquid phase, an fcc ($A1$) phase at both the Al- and Ni-rich ends, a noncongruently melting compound Al_3Ni, and three intermediate phases with a variable range of solubilities Al_3Ni_2, AlNi, and $AlNi_3$.

Several attempts have been made to describe the Ni-Al phase diagram. Kaufman and Nesor[35] have used a subregular solution model to fit experimental thermodynamic data and, with the exception of ordered phases that have been treated as stoichiometric compounds, the overall agreement with the experimental phase diagram is good. This kind of approach has been improved upon by Ansara, Sundman, and Willemin[36] who have used the sublattice model to describe the ordering in Al_3Ni_2, AlNi, and $AlNi_3$ compounds. As already mentioned, Sigli and Sanchez[13] also calculated the phase diagram by describing the thermodynamic behavior of the different phases by CVM; in this case EPI have been determined from experimental thermodynamic data and available phase-diagram information.

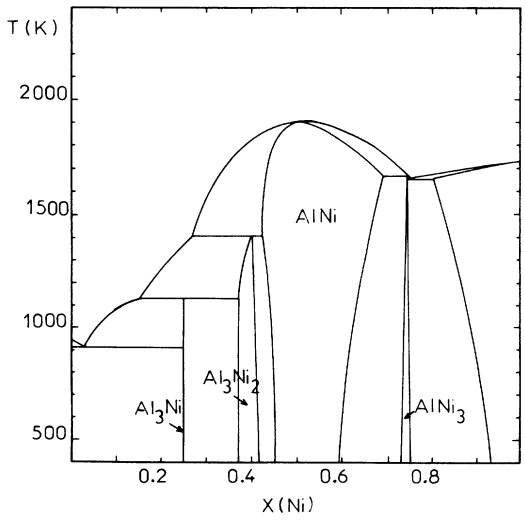

FIG. 1. Experimental phase diagram of the Ni-Al system.

A. Energies of formation of compounds

As a first step, we have calculated the energies of formation of the four intermediate phases observed in the equilibrium phase diagram. In the *structurbericht* notation, these phases are called the $DO_{20}(Al_3Ni)$, $D5_{13}(Al_3Ni_2)$, $B_2(AlNi)$, and $L1_2(AlNi_3)$ phases. The DO_{20} orthorhombic phase is found experimentally to be a stoichiometric compound and is treated as such in the present work. Although the hexagonal $D5_{13}$ phase is experimentally reported to be stable over a small concentration range, it will be described as a stoichiometric compound. To calculate the energies of these two compounds, we have used the tight-binding Hamiltonian described previously, coupled with the recursion method, six exact steps of the continued fraction have been obtained which give 12 exact moments of the electronic density of states; the self-consistency of charge transfer is taken into account via the electron-electron and ion-ion interactions as described in Sec. II A. We obtain -37.0 and -52.1 kJ/atom for Al_3Ni and Al_3Ni_2, respectively.

The $B2$ and $L1_2$ phases are stable over an extended concentration range and are described as SRO phases. We have also used the alloy CBLM to calculate their energies of formation, which are equal to -58.3 and -43.4 kJ/atom, respectively. Calculations of EPI will be discussed in the next section. As the CBLM is exact up to the fourth moment it is essential to check that the results provided by this method are consistent with the results of the recursion method obtained for the stoichiometric Al_3Ni and Al_3Ni_2 compounds. Therefore, we have also performed calculations for AlNi and $AlNi_3$ compounds with the recursion method and obtained -57.4 and -43.1 kJ/atom, respectively; the difference between results obtained in both methods is not significant. Let us mention that it is essential to treat charge transfer in a self-consistent way. All the results and a comparison with experimental data[37] are gathered in Table I.

TABLE I. Energies of formation of the different phases occurring in the Ni-Al system.

	ΔE (kJ/mol)			
	Our work	Ref. 37	Ref. 13	Ref. 47
Al_3Ni	-37	-37.7	-39.8	-21.8
Al_3Ni_2	-52.1	-56.5	-56.5	
AlNi	-57.4	-58.8	-54.5	
$AlNi_3$	-43.1	-41.0	-38.1	-43.1

B. Effective-pair interactions and disordered alloys

EPI's extractions from CBLM calculations for both fcc- and bcc-based structures have been already discussed in Ref. 14 and will not be repeated here. In Table II are compared our EPI values obtained for fcc-based structures to those obtained by Carlsson[38] using a supercell total-energy approach. Values obtained from a fit to the Ni-rich part of the Ni-Al phase diagram based on empirical Lennard Jones potentials[39] are also included. We see that the three sets of data display the same concentration dependence even if our results give smaller values. For all the compositions, the charge transfer comes from Al to Ni; however, it is small as, for instance, the value obtained for the equiatomic composition, $\Delta n_{Ni}=0.14$ electron/atom. This result indicates that the self-consistent contribution from ionic bonding to the formation energies of these alloys is small. In fact, from our calculations[14] and other earlier work,[40,41] strong Ni d and Al p interactions are well established, leading to the existence of a pseudogap which separates the antibonding from bonding and nonbonding regions. This strong hybridization is predominantly important to explain the strong negative values obtained for the formation energies of the compounds or the solid solutions.

For bcc-based structures, only one result given by Sigli and Sanchez[13] can be used for comparison. At 50 at. % Ni, they obtain $4V_1=8.8$ kJ and $3V_2=4.4$ kJ while our values are 6.8 and 0 kJ, respectively. As for fcc-based structures, V_1 and V_2 display a very strong concentration dependence, noting the peculiar behavior of V_2 which displays negative values in the Al-rich part and becomes positive in the Ni-rich end. Once more, the charge transfer is small, $\Delta_{Ni}=0.16$ electron/atom for 50% Ni and very similar to that obtained for the fcc lattice.

In Figs. 2 and 3 are displayed internal energies and free energies of formation calculated at $T=1273$ K for both fcc and bcc structures. Our results are compared to the ones provided by Sigli and Sanchez[13] and also with available experimental data.[37,42] For the fcc structure, the curve obtained by Sigli and Sanchez does not present the same dissymmetry with respect to the equiatomic composition. Our results seem to be more consistent with the fact that the $AlNi_3$ compound crystallizes with the $L1_2$ cubic structure while Al_3Ni compound crystallizes in an orthorhombic structure. However, the values calculated by both methods are in good agreement in the Ni-rich region, where the parameters, used by Sigli and Sanchez, have been fitted with experimental data. For the bcc structure, the agreement between the two sets of calculations is excellent, the comparison with experimental data also being very good.[37,42,43]

TABLE II. Effective-pair interactions for fcc-based structures.

	EPI (kJ/mol)		
x_{Ni}	Our work	Ref. 39	Ref. 47
0.25	2.5	3.9	3.6
0.50	4.4	6.3	5.9
0.75	7.0	8.9	8.2

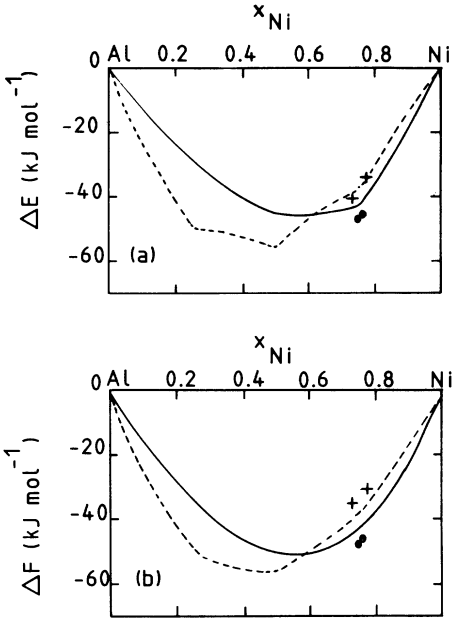

FIG. 2. Internal energies and free energies of formation as a function of composition for fcc lattice ($T=1273$ K); — — —, Ref. 13; +, Ref. 37; ⊙, Ref. 42.

C. Liquid phase

For the liquid phase we present calculations of internal energies at $T=1973$ K and compare our values to the experimental ones;[44,45] two sets of results are presented, one for completely disordered alloys, the other one for equi-

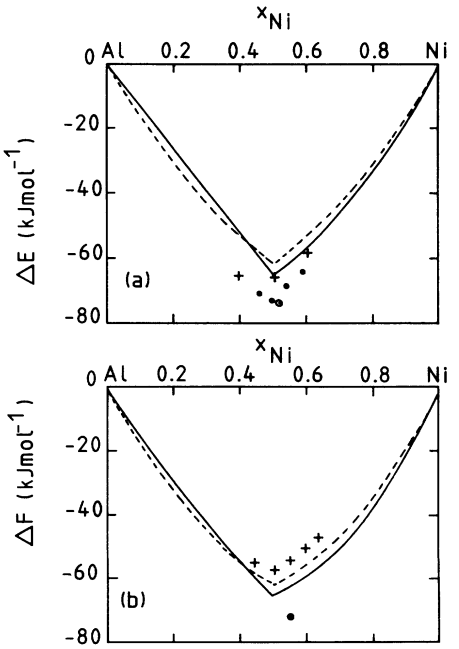

FIG. 3. Internal energies and free energies of formation as a function of composition for bcc lattice ($T=1273$ K). — — —, Ref. 13; +, Ref. 37; ⊙, Ref. 42; ●, Ref. 43.

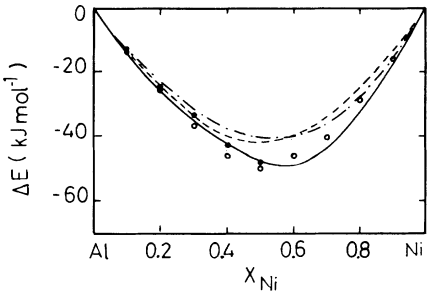

FIG. 4. Internal energies for the liquid phase ($T=1973$ K); ——, with CSRO; —·—·—·, without CSRO; — — —, Ref. 13; ○, Ref. 44; ●, Ref. 45.

librium values of CSRO. We can see that the first curve agrees with Sigli and Sanchez's curve,[13] in agreement with the fact that these authors describe the liquid phase using a subregular solution model. However, from the comparison of our two sets of calculations and experimental data, taking into account CSRO in the liquid phase is essential to obtain a good description of the thermodynamic data of this phase. Ordering effects are maximum around $x_{Ni}=0.6$, which is consistent with the strong concentration dependence of EPI in solid solutions. Strong positive values of EPI in the Ni-rich region result in a strong ordering tendency; for instance the behavior of the $AlNi_3$ compound remains ordered up to its melting point. In the liquid phase, the same effects, though reduced, are observed and shown in Fig. 4.

D. Phase-diagram calculations

We have shown that the tight-binding Hamiltonian coupled with either the CBLM or recursion method is able to reproduce, qualitatively and quantitatively, energies of formation of the different phases occurring in the Ni-Al system. However, to study the equilibrium between these different phases, i.e., the equilibrium phase diagram, there is still a "missing link" in our approach which is the thermodynamic properties of the pure metals or, in other terms, the difference in free energy between the liquid and crystalline phases. At present, such calculations are beyond the scope of our tight-binding calculations and we have chosen to use thermodynamic compilations[46] to obtain these quantities.

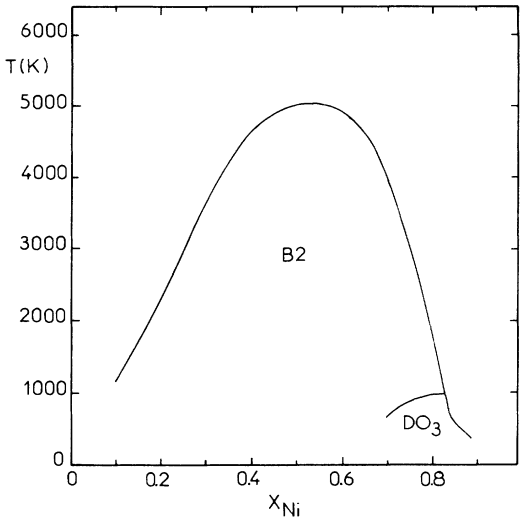

FIG. 6. The bcc Ni-Al phase diagram.

If only fcc-based equilibria are considered, the phase diagram of Fig. 5 is produced. Both $L1_2$ and $L1_0$ phase regions are obtained and all transitions are first order. Only the Ni-rich portion can be directly compared to experimental results since for Ni concentrations less than in the observed Ni_3Al, underlying lattices other than the fcc lattice appear. However, contrary to Carlsson and Sanchez's results,[47] we do not note the presence of a miscibility gap in the metastable Al-rich part. These authors

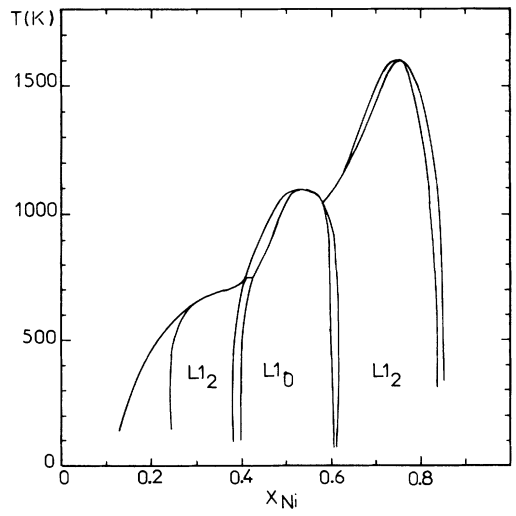

FIG. 5. The fcc Ni-Al phase diagram.

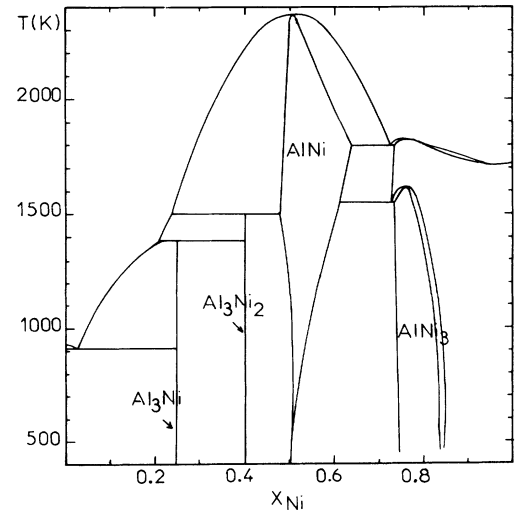

FIG. 7. The calculated Ni-Al phase diagram with a completely chemically disordered liquid.

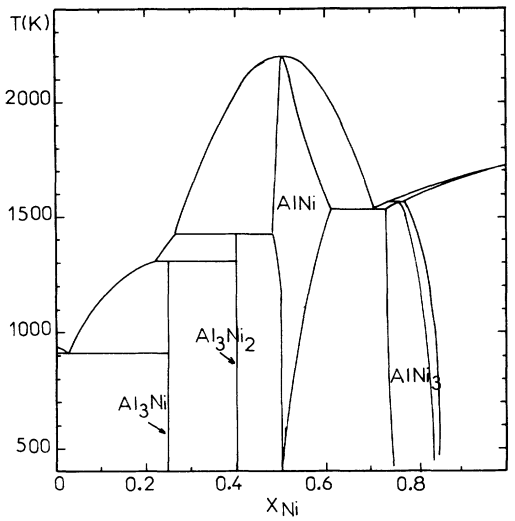

FIG. 8. The calculated Ni-Al phase diagram with chemically short-range-ordered liquid.

explain the origin of this gap from the concentration dependence of the calculated energy of mixing for the completely random fcc solid solutions. Such behavior, i.e., a negative curvature of ΔE_{rand}, was not a result of our work.

The bcc-only phase diagram is shown in Fig. 6. Note that $B2$ disordering takes place at a very high temperature. A DO_3 is expected at high Ni content.

When families of both fcc- and bcc-based free-energy curves are combined with the stoichiometric Al_3Ni and Al_3Ni_2 compounds and the liquid phase, the phase diagram of Fig. 7 is obtained. In this figure, the liquid phase is treated as being completely chemically disordered. In Fig. 8, the same phase diagram is presented but now with the equilibrium values of CSRO of the liquid phase considered. As has already been mentioned, this factor is essential to obtain a good description of the phase diagram. Agreement with the experimental diagram (Fig. 1) is immediately apparent. On the Al side, Al_3Ni and Al_3Ni_2 decompose congruently in the solid state, a central $B2$ phase persists to very high temperatures, and the $L1_2$ phase has a lower disordering temperature. Our calculations lead to a peritectic decomposition of the Ni_3Al compound. The eutectic between the solid phases $NiAl(B2)$,$Ni_3Al(L1_2)$ and the liquid exists to the left of the peritectic, contrary to the usually adopted phase diagrams, but in agreement with the results proposed by Bremer *et al.*[48] It should be noted that the respective positions in the phase diagram of the eutectic and the peritectic are very sensitive to the values of energies of formation of the three concerned phases, i.e., the liquid and the two solids.

V. CONCLUSION

The tight-binding calculation of the Ni-Al system is, in many points, in agreement with experimental observations.

(i) We are able to predict the correct ground states, such as the $B2$ structure being more stable than the $L1_0$ for the equiatomic alloy or the $L1_2$ structure being more stable than the DO_3 structure for the alloy with 75 at. % Ni. The complex orthorhombic DO_{20} structure is also found to be more stable than the fcc- or bcc-based superstructures.

(ii) Taking into account chemical short-range order to describe the free energy of the liquid phase is essential. We find a congruent melting temperature for the NiAl compound higher than the experimental data, but this compound is known to present antisites and vacancies even at the equiatomic composition, factors which are not considered in these calculations. The two complex DO_{20} and $D5_{13}$ structures are found to melt peritectically. For the Al_3Ni compound, the peritectic temperature is some 250 K higher than experiment indicates but for the Al_3Ni_2 compound, it is only 10 K higher than that determined experimentally. From an experimental point of view, the phase boundaries of the peritectic decomposition of the Ni_3Al compound are still controversial. Let us mention that if our results are in agreement with the most recent experimental determinations,[48] they are very sensitive to the values of the energies of the three phases which determine the equilibrium properties.

[1]R. Kikuchi, Phys. Rev. **81**, 998 (1951).
[2]J. W. D. Connolly and A. R. Williams, Phys. Rev. B **27**, 5169 (1983).
[3]L. G. Ferreira, A. A. Mbaye, and A. Zunger, Phys. Rev. B **35**, 6475 (1987).
[4]B. Velicky, S. Kirkpatrick, and H. Ehrenreich, Phys. Rev. **175**, 747 (1968).
[5]A. Gonis and J. W. Garland, Phys. Rev. B **16**, 2424 (1977).
[6]F. Ducastelle and F. Gautier, J. Phys. F **6**, 2039 (1976).
[7]P. E. A. Turchi, G. M. Stocks, W. H. Butler, D. M. Nicholson, and A. Gonis, Phys. Rev. B **37**, 5982 (1988).
[8]F. Ducastelle, in *Alloy Phase Stability, Proceedings of the 1987 MRS NATO Advanced Study on Alloy Phase Stability,* edited by A. Gonis and G. M. Stocks (Kluwer Academic, Boston, 1989), p. 293.
[9]M. D. Robbins and L. M. Falicov, Phys. Rev. B **28**, 1333 (1984).
[10]M. Sluiter, P. E. A. Turchi, Fu Zehong, and D. de Fontaine, Phys. Rev. Lett. **60**, 716 (1988).
[11]M. O. Robbins and L. M. Falicov, Phys. Rev. B **25**, 2343 (1982).
[12]D. Mayou, D. Nguyen Manh, A. Pasturel, and F. Cyrot-Lackmann, Phys. Rev. B **33**, 3384 (1986).
[13]C. Sigli and J. M. Sanchez, Acta Metall. **33**, 1097 (1985).
[14]C. Colinet, A. Bessoud, and A. Pasturel, J. Phys. Condens. Matter **1**, 5837 (1989).
[15]D. Nguyen Manh, D. Mayou, A. Pasturel, and F. Cyrot-Lackmann, J. Phys. F **15**, 1911 (1985).

[16]A. Pasturel, D. Nguyen Manh, and D. Mayou, J. Phys. Chem. Solids **47**, 325 (1986).
[17]F. Gautier, J. Van der Rest, and F. Brouers, J. Phys. F **5**, 1884 (1975).
[18]M. O. Robbins and L. M. Falicov, Phys. Rev. B **29**, 1333 (1984).
[19]R. Haydock, in *Solid State Physics,* edited by H. Erhenreich, D. Turnbull, and F. Seitz (Academic, New York, 1980), Vol. 35, p. 215.
[20]M. Maret, T. Pomme, A. Pasturel, and P. Chieux, Phys. Rev. B **42**, 1598 (1990).
[21]A. Pasturel, J. Hafner, and P. Hicter, Phys. Rev. B **32**, 5009 (1985).
[22]J. Hafner, G. Kahl, and A. Pasturel, in *Liquid and Amorphous Materials,* edited by E. Lüscher and G. Fritsch, NATO Advanced Study Institute Series E (Sitjhoff and Noerdholf, Alpen Van Rijn, 1987), p. 164.
[23]A. Pasturel and J. Hafner, Phys. Rev. B **34**, 8357 (1986).
[24]A. Pasturel, unpublished results.
[25]W. A. Harrison, in *Electronic Structure and the Properties of Solids,* edited by W. H. Freeman (Freeman, San Francisco, 1980).
[26]H. Shiba, Prog. Theor. Phys. **46**, 77 (1971).
[27]F. Herman and S. Skillman, in *Atomic Structure Calculations* (Prentice-Hall, Englewood Cliffs, NJ, 1965).
[28]S. Froyen, Phys. Rev. B **27**, 7194 (1980).
[29]R. Kikuchi and H. Sato, Acta Metall. **22**, 1099 (1974).
[30]R. Kikuchi, J. Chem. Phys. **60**, 1071 (1974).
[31]R. Kikuchi and D. de Fontaine, Natl. Bur. Stand. (U.S.) Report No. P-496, 1978, p. 967.
[32]M. S. Wertheim, Phys. Rev. Lett. **10**, 321 (1963).
[33]E. Waisman, J. Chem. Phys. **59**, 495 (1973).
[34]R. Kikuchi and J. Murray, Calphad **9**, 311 (1985).
[35]L. Kaufman and H. Nesor, Calphad **2**, 325 (1978).
[36]I. Ansara, B. Sundman, and P. Willemin, Acta Metall. **36**, 977 (1988).
[37]R. Hultgren, P. D. Desai, D. T. Hawkins, M. Gleiser, and K. K. Kelly, *Selected Values of the Thermodynamic Properties of Binary Alloys* (American Society for Metals, Metals Park, OH, 1973).
[38]A. E. Carlsson, Phys. Rev. B **35**, 4858 (1987).
[39]C. Sigli and J. M. Sanchez, Calphad **8**, 221 (1984).
[40]D. Hackenbracht and J. Kubler, J. Phys. F **10**, 427 (1980).
[41]C. D. Gelatt, A. R. Williams, and V. L. Moruzzi, Phys. Rev. B **27**, 2005 (1983).
[42]V. M. Es'kov, V. V. Samskhval, and A. A. Vecher, Izv. Akad. Nauk SSSR Met. **2**, 199 (1974).
[43]E. T. Henig and H. L. Lukao, Z. Metallkd. **66**, 98 (1975).
[44]V. M. Sandakov, Yu O. Esin, and P. V. Gel'd, Russ. J. Phys. Chem. **45**, 1020 (1971).
[45]N. V. Gizenko, S. N. Kilesso, D. V. Ill'Inkov, B. I. Emlin, and A. L. Zav'yalov, Sov. J. Non-Ferrous Met. **4**, 263 (1983).
[46]A. T. Dinsdale (unpublished).
[47]A. E. Carlsson and J. M. Sanchez, Solid State Commun. **65**, 527 (1988).
[48]F. J. Bremer, M. Beyss, E. Karthaus, A. Hellevig, T. Schober, J. M. Welter, and H. Wenzl, J. Cryst. Growth **87**, 185 (1988).